# Overcoming Low mRNA Expression in White Matter: A Protocol for RNA Extraction From the Optic Nerve in Large Animals for Transcriptomic Analysis

Zhonghao Yu,[1,2] Yue Guan,[1,2] Tian Xia,[1,2] Xuanwen Li,[1,2] Mingyue Liu,[1,2] Yujia Huo,[1,2] Zhuowei Wang,[1,2] Zhirong Liu,[1,2] Yuting Luo,[1,2] Wentao Yan,[1,2] Lanfang Sun,[1,2] Wencan Wu,[1–3] Baoguo Shen,[1,2] and Yikui Zhang[1,2]

[1]The Eye Hospital, School of Ophthalmology and Optometry, Wenzhou Medical University, Wenzhou, Zhejiang, China
[2]State Key Laboratory of Ophthalmology, Optometry and Vision Science, Eye Hospital, Wenzhou Medical University, Wenzhou, China
[3]Oujiang Laboratory (Zhejiang Lab for Regenerative Medicine, Vision, and Brain Health), Wenzhou, Zhejiang, China

Correspondence: Yikui Zhang, The Eye Hospital, School of Ophthalmology and Optometry, Wenzhou Medical University, 270 West Xueyuan Road, Wenzhou, Zhejiang 325027, China; zhang.yikui@wmu.edu.cn.
Baoguo Shen, The Eye Hospital, School of Ophthalmology and Optometry, Wenzhou Medical University, 270 West Xueyuan Road, Wenzhou, Zhejiang 325027, China; shenbaoguo@wmu.edu.cn.
Wencan Wu, The Eye Hospital, School of Ophthalmology and Optometry, Wenzhou Medical University, 270 West Xueyuan Road, Wenzhou, Zhejiang 325027, China; wuwencan@wmu.edu.cn.

ZY, YG, TX, and XL contributed equally to this work.

**Received:** May 15, 2024
**Accepted:** October 21, 2024
**Published:** November 14, 2024

Citation: Yu Z, Guan Y, Xia T, et al. Overcoming low mRNA expression in white matter: A protocol for RNA extraction from the optic nerve in large animals for transcriptomic analysis. *Invest Ophthalmol Vis Sci.* 2024;65(13):25. https://doi.org/10.1167/iovs.65.13.25

**Purpose.** White matter (WM) abnormalities are associated with various central nervous system (CNS) disorders, and the optic nerve provides a unique opportunity to study WM pathology. Large animal models offer a more suitable platform for preclinical testing of novel therapeutic strategies for optic neuropathy due to their similarities to humans in size and relevant anatomy. Transcriptomic analyses of optic nerve tissue are essential for understanding the underlying pathological mechanisms. However, extracting high-quality RNA from the optic nerve in large animals remains challenging.

**Methods.** We utilized in situ hybridization and single-nucleus RNA sequencing (snRNA-seq) to examine mRNA expression in WM cells and gray matter (GM) cells.

**Results.** We discovered that mRNA expression levels in WM cells were only 15% to 66% of those in GM neurons. To overcome the low mRNA yield, we developed a specialized RNA extraction protocol for the intra-canalicular optic nerve in large animal models, achieving an RNA integrity number (RIN) of 6.8 ± 0.06. For single-cell transcriptomics (scRNA-seq), we obtained a cell density of $1.0 \times 10^5$ cells/µL, cell viability of 93% ± 1.84%, and an agglomeration rate of 5.37% ± 0.75%. This approach is also applicable for postmortem human optic nerve with a RIN of 8.3 ± 0.3 using snRNA-seq.

**Conclusions.** We first discovered that the mRNA expression in the WM was significantly lower than that in the GM. Our RNA extraction protocol from large animal models enhances transparency and reproducibility in transcriptomic studies of optic nerve and other WM tissues.

Keywords: mRNA expression, white matter (WM) (optic nerve), gray matter (GM), large animals, multi-transcriptomic techniques

The white matter (WM) in the central nervous system (CNS) is composed of nerve fibers that enable communication between CNS neurons. Abnormalities in the WM can lead to CNS dysfunction and are often observed in the early stages of CNS trauma, such as traumatic brain injury.[1,2] The optic nerve provides a suitable platform for WM-related studies because it consists of axonal nerve fibers derived from retinal ganglion cells (RGCs) and lacks any grey matter (GM).

Moreover, optic neuropathy is a leading cause of irreversible blindness worldwide.[3,4] Although there have been significant breakthroughs in strategies for repairing the optic nerve derived from small animal models, effective clinical treatments for optic neuropathies in humans remain extremely limited. We previously reported that goats and rhesus macaques have a human-like nasal cavity and sphenoid sinus, and that their optic canal and optic chiasm can be accessed and modulated micro-invasively using clinical trans-nasal endoscopy,[5] making them suitable animal models for preclinical tests of novel therapeutic strategies.

To explore the pathological mechanisms underlying optic neuropathy, transcriptomic analyses, such as bulk

RNA sequencing (RNA-seq), single-cell RNA-seq, and spatial sequencing of the optic nerve tissue were required. The extraction of high-quality RNA from the optic nerve for transcriptomic analysis presents considerable challenges in large animals. First, the housing environment for large animals tends to be less sterile than that for small animals. Consequently, there is potentially a higher prevalence of RNase contamination from microorganisms residing on the skin and fur of large animals. Second, harvesting tissue from large animals is more time-consuming than that from small animals, leading to more RNA degradation during tissue harvesting.[6] Third, due to the deep location of the optic nerve in the orbit or at the base of the skull, harvesting is also more time-consuming, increasing the risk of contamination from RNases in other neighboring tissues.

To overcome these challenges, we developed a reliable protocol for RNA extraction from the intra-canalicular optic nerve in large animal models. Using this protocol, we successfully identified transcriptomic changes associated with optic canal crush injuries that were predominantly enriched in pathways related to inflammation, ischemia, and metabolism.[5]

## Methods

### Human Optic Nerve

The human tissue experiments complied with the guidelines of the ARVO Best Practices for Using Human Eye Tissue in Research (November 2021). This study was approved by the Ethics Committee of the Eye Hospital affiliated with Wenzhou Medical University (Approval No: 2022-120-K-91). After the donor's cardiac death, the whole eyeball was removed within 1 hour, the retrobulbar optic nerve was quickly cut out, loaded into a 1.5 mL EP tube, and quickly thrown into liquid nitrogen and kept under dry ice during shipping.

### Animals

All experiments were conducted in compliance with the ARVO Statement for the Use of Animals in Ophthalmic and Vision Research approved by Wenzhou Medical University (rat approval no: YSG24042803 and goat approval no: wydw2020-0789), involved 2-month-old male Wistar rats from Beijing Vital River Laboratory and 6-month-old male Saanen goats from Caimu Livestock. All were housed in the animal facility of Wenzhou Medical University under a 12-hour light/dark cycle with unrestricted food and water.

### Reagents and Instruments

All materials and supplies are listed in Tables 1 through 4, according to their use in dissection, harvest, and sequencing processes.

### Cryo-Embedded Tissue Section Preparation

Rats were euthanized with $CO_2$ and then transcardially perfused with 4% paraformaldehyde (PFA). Goat's brain and optic nerve samples were fixed in 4% PFA, cryoprotected in 0.1 M phosphate buffer containing 30% sucrose, frozen with optimum cutting temperature (OCT) compound, and sectioned at a thickness of 10 µm. Further processing of the sections is detailed in the published paper.[7]

### mRNA and Neuron Detection in the Optic Nerve and Cortex With $\pi$-FISH

The in situ hybridizations were carried out as described previously[7] and the specific probes for the target goat *Rbfox3* (accession number = XM_018063660.1) were designed by spatial FISH company. After dehydration and denaturation of the slides with methanol, hybridization buffer with specific targeting probes was added to the chamber for incubation at 37°C overnight. Then, the slides were washed 3 times with PBST, followed by ligation of the target probes in ligation mix at 25°C for 3 hours. Next, the slides were washed 3 times with PBST and subjected to rolling circle amplification with phi29 DNA polymerase at 30°C overnight. Fluorescent detection probes in hybridization buffer were applied to the slides. Finally, the slides were dehydrated with an ethanol series and mounted with mounting medium. Images were acquired using a Thunder Imager 3D microscope.

### RNA Degradation Assay

The PFA-fixed slides were dehydrated and denatured using 100% methanol. Subsequently, 0.4 mg/mL RNase A was added, and the samples were incubated at 37°C for 2 hours to enzymatically digest the RNA. Next, the slides were washed with PBST for 2 minutes each, and this process was repeated 3 times. After the washing steps, 0.1 µM oligo-dT containing the Cy5 modification was added to the reaction chamber. The mixture was incubated at 37°C for 30 minutes, followed by a subsequent 30 minutes of incubation at room temperature. The slides were washed again with PBST for 5 minutes per wash and incubated at room temperature for an additional 30 minutes. Images were acquired using a Thunder Imager 3D microscope.

### Quantitative and Statistical Analyses of *Rbfox3* and mRNA Poly(A) Expression

We applied the freehand selection or threshold function of ImageJ (https://imagej.nih.gov/ij/) to circle cells co-stained with DAPI and *Rbfox3*, colocalized the circled areas into the poly(A) monochrome channel, and calculated the average fluorescence brightness of the circled areas. Statistical analyses were performed using GraphPad Prism 8. Prior to analysis, the residuals of the data were subjected to normality and homogeneity of variance tests. For comparisons between more than 2 groups, we used ordinary 1-way ANOVA followed by Tukey's multiple comparisons test. For comparisons between the two paired groups, a paired *t*-test was used, whereas for the unpaired groups, an unpaired *t*-test was used.

### Single-Nucleus RNA-Seq Data Analysis

The processing of raw data is detailed in the Supplementary Data. The cell-by-gene count matrices were converted to Seurat version 5 objects. Cells with RNA counts less than 300 or greater than 6000 were filtered out as low-quality cells. Additionally, cells with mitochondrial fractions greater than 20% were removed. Clustering, visualization, and cell type annotation of single-nucleus RNA sequencing (snRNA-seq) data.

Two samples of GM and WM were first integrated using Seurat integration functions. Data scaling, dimensional

Investigative Ophthalmology & Visual Science

**Table 1.** Key Resources Table

| Number | Name | Source | Identifier |
|---|---|---|---|
| *Instrument* | | | |
| 1 | Shaver | Codos (Shenzhen, China) | CP-9200 |
| 2 | Knife blade | Lianhui (Shanghai, China) | / |
| 3 | Knife handle | JZ Classic (Shanghai, China) | J11010 |
| 4 | Needle holder | JZ Classic (Shanghai, China) | J32020 |
| 5 | Hack saw blade (24T) | Bahco (Wisconsin, USA) | SANDFLEX |
| 6 | Kidney tray | JZ Classic (Shanghai, China) | R0B020 |
| 7 | Ophthalmic forceps | Xiehe Medical Instruments (Jiangsu, China) | MR-F423 |
| 8 | Eye scissors | Xiehe Medical Instruments (Jiangsu, China) | MR-S232-3 |
| 9 | Brain spatula | JZ Classic (Shanghai, China) | NAE200 |
| 10 | Hack saw | Deli Group (Zhejiang, China) | DL6001 |
| 11 | Tin paper embedding box | / | / |
| 12 | Medical gauze swab | Zhende (Zhejiang, China) | 20211210 |
| 13 | Injectors (1 and 20 ml) | Kangdelai (Shanghai, China) | / |
| 14 | EP tubes (1.5 ml) | Jet BioFil (Guangzhou, China) | CFT001015 |
| 15 | Surgical trays (226*144*45 mm) and stainless-steel bowl | / | / |
| 16 | Paper towels | / | / |
| 17 | Tin foil | / | / |
| 18 | Petri dish | Corning (New York, USA) | 353001 |
| 19 | Marker pen | / | / |
| 20 | Parafilm sealing film | Stellar Scientific (Maryland, USA) | IL.60631 |
| 21 | Medical cotton balls | AiHuJia (Jiangsu, China) | / |
| 22 | Closed IV catheter system | BD Medical Devices (New Jersey, USA) | 383019 |
| 23 | Disposable drape | Zhende (Zhejiang, China) | / |
| 24 | Centrifuge tubes (50 ml) | Corning (New York, USA) | 430290 |
| 25 | Thunder Imager 3D microscope | Leica (Wetzlar, Germany) | DMi8 |
| *Reagent* | | | |
| 26 | OCT compound | Sakura (California, USA) | 4583 |
| 27 | MACS tissue storage solution | Miltenyi Biotec (North Rhine-Westphalia, Germany) | 130-100-008 |
| 28 | Diethyl pyrocarbonate | Sigma Aldrich (St. Louis, Missouri, and Germany) | BCCD0386 |
| 29 | RNase Knockout | Fujifilm Corporation (Tokyo, Japan) | 181-03381 |
| 30 | Gene Keeper RNA & DNA stabilization solution | Fujifilm Corporation (Tokyo, Japan) | 319-08901 |
| 31 | PBS (DEPC-treated) | Servicebio (Hubei, China) | G0002 |
| 32 | Physiological saline | / | / |
| 33 | Medical-grade alcohol | / | / |
| 34 | Dry ice | / | / |
| 35 | Liquid nitrogen | / | / |
| 36 | NeuN | Proteintech (Hubei, China) | 66836-1-lg |
| 37 | Phi29 | New England Biolabs (Massachusetts, USA) | M0269S |
| 38 | RNase A | Takara (Tokyo, Japan) | 2158 |
| 39 | Collagenase | Sigma Aldrich (St. Louis, Missouri, and Germany) | C0130-1G |
| 40 | Trypsin | Gibco (New York, USA) | 154000-054 |

**Table 2.** Dissection Equipment Kit

| Number | Name | Sterilized | Function |
|---|---|---|---|
| 1 | Shaver | No | To remove hair |
| 2 | Knife blade | Yes | To remove Skin |
| 3 | Knife handle | No | |
| 4 | Needle holder | No | |
| 5 | Hack saw blade (24T) | No | Used with hack saw |
| 6 | Hack saw | No | To remove the cranial parietal bones of goats |
| 8 | Kidney tray | No | To hold large animal heads |
| 9 | PBS (DEPC-treated) | Yes | To rinse large animal heads |

reduction, and clustering were then performed on the integrated dataset using the standard Seurat pipeline. For visualization, combined UMAPs were generated using the first 10 dimensions.

The cluster identity was assigned based on the expression of the following well-defined marker genes[8,9]: oligodendrocytes (Mbp and Mobp), astrocytes (Plpp3, Gja1, Gfap, and Aqp4), oligodendrocyte precursor cells (Vcan, Tnr, and Pdgfra), microvascular cells (Cst3, Cx3cr1, and Hexb), glutamatergic neurons (Slc17a7 and Camk2a), GABAergic neurons (Gad1 and Gad2), SST INs (Sst, Gad1, and Gad2), and PV INs (Cntnap4, Gad1, and Gad2).[8]

**Table 3.** Sample Harvesting Equipment

| Number | Name | Sterilized | Function |
|---|---|---|---|
| 1 | Ophthalmic forceps | Yes | To expose the optic nerve |
| 2 | Eye scissors | Yes | |
| 3 | Needle holder | Yes | |
| 4 | Knife blades | Yes | |
| 5 | Knife handle | Yes | |
| 6 | Brain spatula | Yes | To mobilize the delicate brain parenchyma |
| 7 | Paper towels | Yes | To remove the water from the tissue |
| 8 | Disposable drape | Yes | To prevent contamination of the operation area |
| 9 | Surgical trays (226*144*45 mm) | Yes | To contain surgical equipment |

**Table 4.** Multi-transcriptomic Sequencing Equipment

| Number | Name | Sterilized | Function |
|---|---|---|---|
| Bulk RNA-sequencing kit | | | |
| 1 | EP tubes | Yes | To collect samples |
| 2 | Parafilm sealing film | No | To seal EP tubes |
| 3 | PBS (DEPC-treated) | Yes | To wash blood off samples |
| 4 | RNase Knockout | / | To reduce residual RNases |
| 5 | Liquid nitrogen | / | To freeze samples |
| 6 | Gene Keeper RNA and DNA stabilization solution | / | To protect RNA degeneration |
| Single-cell RNA sequencing kit | | | |
| 1 | Parafilm sealing film | No | To seal EP tubes |
| 2 | EP tubes | Yes | To collect samples |
| 3 | MACS tissue storage solution | / | To store fresh samples |
| 4 | Physiological saline | Yes | To remove blood from samples |
| Spatial sequencing kit | | | |
| 1 | Tin paper embedding box | Yes | To store samples with OCT |
| 2 | Diethyl pyrocarbonate | / | To prepare DEPC-treated PBS |
| 3 | PBS (DEPC-treated) | Yes | To wash blood from samples |
| 4 | Injector | Yes | To remove bubbles from OCT |
| 5 | Sterile gauze | Yes | To remove excess liquid |
| 6 | Centrifuge tube | Yes | To prevent samples |
| 7 | Tin foil | No | To protect samples |
| 8 | Petri dish | Yes | / |
| 9 | Ophthalmic forceps | Yes | To adjust sample position |
| 10 | Marker pen | No | / |
| 11 | Dry ice | / | To freeze samples |
| 12 | OCT compound | / | To embed samples |

## Results

### mRNA Expression in White Matter is Significantly Lower Tan That in Gray Matter

We used a specific probe for the *Rbfox3* gene, which encodes the neuronal marker NeuN, to identify neurons in a goat's brain.[10,11] By using fluorescence in situ hybridization ($\pi$-FISH), we examined the expression levels of *Rbfox3* and the poly(A) tail (total mRNA) in both neuron and non-neuron cells (Fig. 1A). We confirmed that the *Rbfox3* probe had the same expression pattern as the anti-NeuN antibody (Supplementary Fig. S1A).

To assess the temporal correlation between the poly(A) tail and mRNA expression,[12] we conducted an RNA degradation assay and observed that after 2 hours of treatment with RNase A, we could hardly detect any mRNA in the treated brain tissue, but untreated samples still exhibited a robust mRNA signal, suggesting the poly(A) tail level accurately reflects mRNA expression at the examined timepoint (Supplementary Fig. S1B).

We subsequently examined the expression levels of *Rbfox3* and the poly(A) tail in the goat's cortex and optic nerve. We found that the GM exhibited higher mRNA expression, as indicated by stronger poly(A) tail fluorescence, compared to the WM in the goat cortex. The primary contributors to this mRNA expression were *Rbfox3*+ neuronal cells (Figs. 1B–E). Interestingly, due to the lack of neuronal cells in the optic nerve, its mRNA expression was significantly lower than that in GM neurons (Figs. 1F, 1G).

Similar heterogeneity of mRNA expression levels between GM and WM tissues was observed in various regions of the CNS in rats, including the spinal cord, brain, and retina. In the spinal cord, we found higher mRNA expression level in *Rbfox3*+ neuronal cells in the GM compared to *Rbfox3*– non-neuronal cells in either the GM or WM (Figs. 2A, 2B). Similarly, we found that the cells in the GM exhibited significantly higher mRNA expression than those in the WM, in both the cortex and the hippocampus (Figs. 2C, 2E). Consistently, RGCs in the retina expressed higher mRNA levels than optic nerve cells (Figs. 2D, 2F). Notably, the sclera and optic nerve of displays strong fluorescence intensity in the extra-

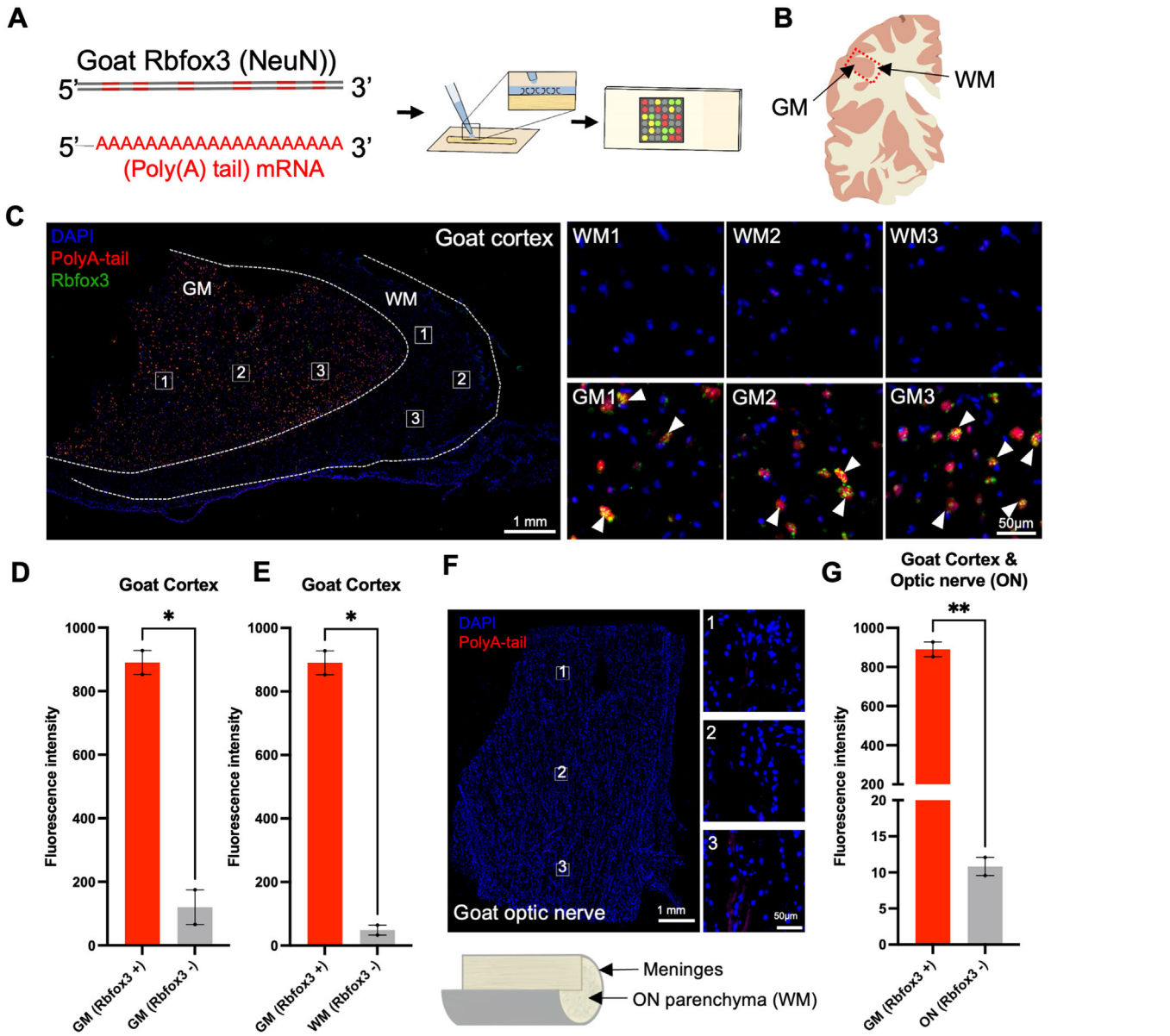


**Figure 1.** In situ hybridization of *Rbfox3* and the poly(A) tail in the goat cortex, goat optic nerve, and rat spinal cord. (**A**) Schematic illustration of the $\pi$-FISH technique. The *red line* and *red text* indicate *Rbfox3*- and poly(A) tail-targeting sequences, respectively. (**B**) Schematic diagram of the cerebral cortex of a sheep. (**C**) Double-fluorescence in situ hybridization trial in the goat cortex using specific probes for *Rbfox3* and poly(A) tails. The landmarks indicate white matter (WM) and gray matter (GM). Scale bars represent 1 mm. Representative images of GM and WM in the selected area are shown on the right. The *arrowhead* indicates co-expression of *Rbfox3* and the poly(A) tail. Scale bars represent 50 μm. (**D, E**) Quantitative analyses of florescence in the goat cortex (**C**). Error bars indicate the standard error. Significance scores represent *P* values of paired *t*-test (*, $P < 0.05$). (**F**) *Upper panel*, double-fluorescence in situ hybridization trial of the goat optic nerve (ON) using specific probes for *Rbfox3* and poly(A) tails. Scale bars represent 1 mm; *bottom panel*, schematic diagram of the goat optic nerve. Representative images of ON in the selected area are shown on the right. Scale bars represent 50 μm. (**G**) Quantitative analyses of florescence in the goat cortex and optic nerve (**C** and **F**). Significance scores represent *P* values of unpaired *t*-test (**, $P < 0.01$).

cellular matrix (see Fig. 2D), likely due to collagen-binding nonspecific signals.[13]

To validate these $\pi$-FISH staining results, we conducted snRNA-seq on the rat cortex, which contains both WM and GM. We identified eight cell types: four glial cell types (oligodendrocytes, astrocytes, oligodendrocyte precursor cells, and microglia) and four types of neurons (glutamatergic neurons, GABAergic neurons, somatostatin inhibitory neurons, and parvalbumin inhibitory neurons; Figs. 3A–C). We found that each neuronal cell type had significantly higher average n-count RNA than the non-neuronal cell types (glial cells; Fig. 3D). Besides, the neuron marker *Rbfox3* was more present in neurons, which matches our staining results (see Fig. 2C, Fig. 3E). Consistently, snRNA-seq data from the retina and optic nerve of goats also supported these findings: each neuronal cell type in the retina exhibited higher n-count RNA values compared to either retinal glial cells or optic nerve cells (Fig. 3F, Supple-

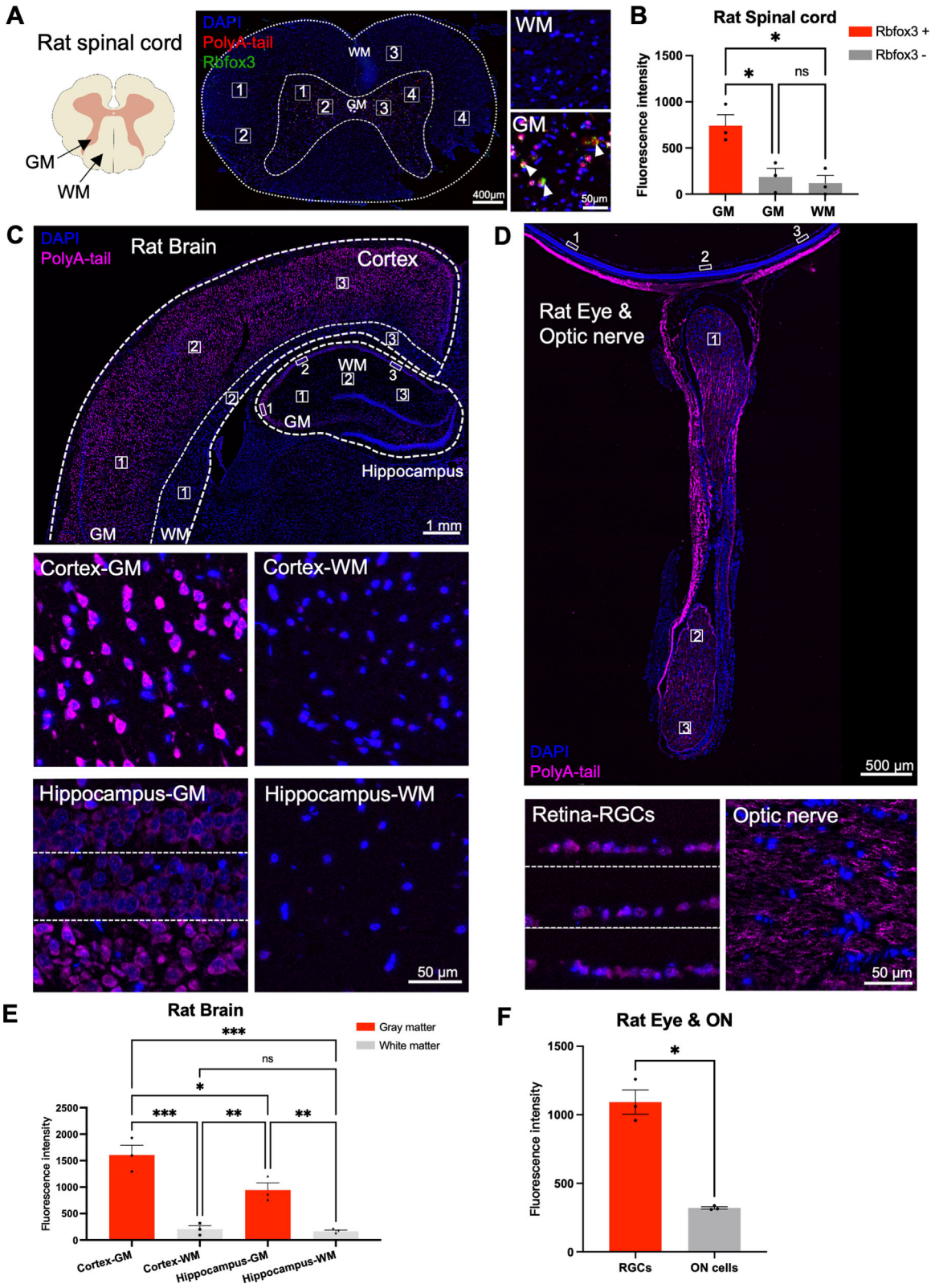


**Figure 2.** Fluorescence in situ hybridization of the poly(A) tail in the rat cortex, hippocampus, eye, and optic nerve. (**A**) *Left panel*, schematic diagram of the rat spinal cord; *right panel*, double-fluorescence in situ hybridization trial of the rat spinal cord using specific probes for *Rbfox3* and poly(A) tails. Scale bars represent 400 µm. Representative images of GM and WM are shown on the right. The *arrowhead* indicates co-expression of *Rbfox3* and the poly(A) tail. Scale bars represent 50 µm. (**B**) Quantitative analyses of florescence in the rat spinal cord (**A**). Error bars indicate the standard error. Significance scores represent *P* values of ordinary 1-way ANOVA with Tukey's multiple comparisons test (*, $P < 0.05$, **, $P < 0.01$, NS, nonsignificant, $P > 0.05$). (**C**) Fluorescence in situ hybridization assay in rat brain using poly(A) tail-specific probes. The landmarks indicate white matter (WM) and gray matter (GM) in the cortex and hippocampus. Scale bars represent 1 mm.

Representative images of WM and GM in the cortex and hippocampus are shown below. Scale bars represent 50 µm. (**D**) Fluorescence in situ hybridization assay in the rat eye and optic nerve using poly(A) tail-specific probes. Scale bars represent 500 µm. Representative images of retina RGCs layer and optic nerve are shown below. Scale bars are 50 µm. (**E**) Quantitative WM and GM fluorescence analysis in rat brain cortex and hippocampus. Error bars indicate the standard error. The ***P*** values for significance scores are from ordinary 1-way ANOVA with Tukey's multiple comparisons test (*, $P < 0.05$; **, $P < 0.01$; ***, $P < 0.001$; NS, not significant, $P > 0.05$). (**F**) Quantitative fluorescence analysis in the rat eye and optic nerve. Error bars indicate the standard error. The ***P*** values for significance scores are from paired ***t***-test (*, $P < 0.05$).

mentary Fig. S2). Given the low mRNA expression level in the WM, a suitable procedure for tissue harvesting and RNA extraction from the WM (optic nerve), especially in large animals, was required.

## Detailed Procedure for Tissue Harvesting and RNA Extraction From the Optic Nerve in Large Animals

(1) Tool preparation.
The tools required for optic nerve exposure and sampling are shown in Figures 4A and 4B and detailed in Tables 2 and 3. These tools were sterilized at 121°C for 60 minutes, soaked in DEPC-treated water overnight, and re-sterilized at 121°C for 30 minutes before use. Notably, the tools required for optic nerve exposure can be used across different goats, whereas the tools needed for optic nerve sampling should be used exclusively for a single large animal. This precaution helps prevent potential RNase contamination and RNA cross-contamination among large animals.

(2) Animal euthanasia.
The goats were euthanized by an injection of 20 mL of 10% potassium chloride solution (KCl, 100 mg/mL) after being anesthetized with xylazine (3 mg/kg) and 3% isoflurane (2 L/min).

(3) Dissection of the optic nerve and retina (Figs. 4C, 4D, Supplementary Video).

(3.1) Following euthanasia, the goat's neck was shaved to expose the carotid artery.

(3.2) The carotid artery was cut with a scalpel to release the blood.

(3.3) The skin and muscles in the neck were cut to expose the cervical vertebrae, which was then sawed to separate the head from the body.

(3.4) The skin and the subcutaneous tissue over the skull were removed using a needle holder and scalpel, and then the skull was flushed with DEPC-treated PBS (see Fig. 4C).

(3.5) The skull roof and part of the brain tissue were sawed off, first vertically along the frontal bone above the upper rim of the orbit, and then horizontally from the occipital bone until the skull roof could be manually removed (see Fig. 4C, right panel).

(3.6) The exposed skull was placed on a UV-sterilized ultraclean table that had been wiped with RNase Knockout solution.

Potential risks and troubleshooting tips: the first saw line should be positioned slightly above the entire orbit, ensuring it is neither too far, to avoid excessive residual bone, nor too close, to prevent damage to the optic nerve or optic chiasm (see Fig. 4C).

(4) Harvesting the optic nerve and retina for RNA sequencing (Fig. 5, Supplementary Video).

(4.1) Materials and tools needed for tissue harvesting are shown in Figure 5A. According to our practice, the tools for tissue exposure were placed to the left of the exposed skull and those for tissue harvesting were placed to the right (see Fig. 5B).

(4.2) The exposed skull was covered with a disposable surgical drape, ensuring that only the sampling area remained visible (see Fig. 5B).

(4.3) A brain spatula was used to lift the frontal cortex to expose the olfactory nerves, which was then cut by ophthalmic scissors.

(4.4) We continued to lift the frontal cortex to expose the underlying optic chiasm, and then cut the bilateral optic tracts.

(4.5) The anterior brain tissue was removed to fully expose the anterior and middle skull base (see Fig. 5C).

(4.6) The periosteum covering the skull base bone was removed using toothed forceps and a scalpel (see Fig. 5D).

(4.7) To expose the intra-orbital and intra-canalicular optic nerve, the upper walls of the orbit and optic canal were carefully removed piece by piece using a needle holder (see Fig. 5D).

(4.8) To harvest the intra-canalicular optic nerve, we cut the intra-cranial segment of the optic nerve, then carefully separated the intra-canalicular optic nerve from the optic canal by either blunt dissection with a fine periosteal elevator or sharp cutting with a scalpel. To harvest the intra-orbital optic nerve, we removed the overlying orbital tissue and the surrounding extraocular muscles using toothed forceps and ophthalmic scissors. The harvested optic nerve was rinsed in DEPC-treated PBS for 1 to 2 seconds to avoid RNase contamination. To harvest the retina, an eyecup was created by removing the cornea and lens. It was then cut into a four-leaf clover shape using ophthalmic scissors. The vitreous humor was carefully removed by scraping with a blunt handle end of a scalpel, and the underlying retinal tissue was delicately collected.

(4.9) We used various kits to store the tissue for different transcriptomic analyses, optimizing the preservation conditions (Figs. 6A, 6C, 6E, Table 4). For both bulk RNA-seq and snRNA-seq, samples were rapidly frozen in liquid nitrogen and shipped on dry ice (Fig. 6B). For single-cell RNA sequencing, we stored the samples in MACS Tissue Storage Solution and shipped them at 4°C to sequencing companies (Fig. 6D). For spatial sequencing, samples were placed in a tin foil embedding box (Fig. 6G), and the embedding box was filled with OCT compound, which solidified on dry ice (Fig. 6F). Once the OCT had solidified, the sample orientation was marked. The embedded samples were placed in 50 mL centrifuge tubes and shipped on dry ice to the sequencing company (see Fig. 6F).

Investigative Ophthalmology & Visual Science

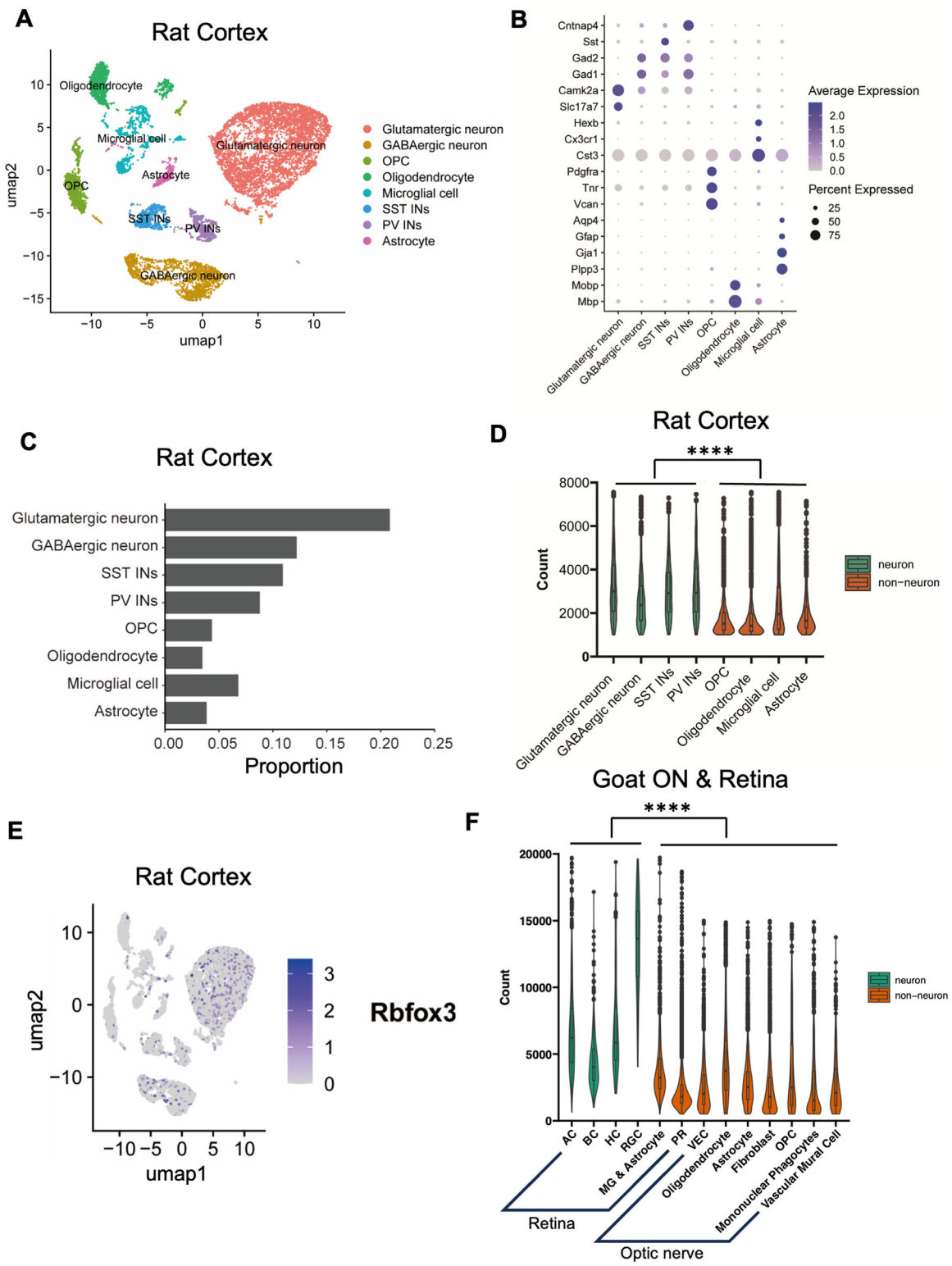


**Figure 3.** Single-nucleus transcriptomic analysis of rat cortex and goat retina and optic nerve. (**A**) UMAP visualization of high-quality rat cortex cells. (**B**) Dot plot showing the marker genes of each cell type in rat cortex sequencing data. (**C**) Bar plot showing the proportion of rat cortex cells in each cluster. (**D**) Violin plots showing the n-counts-RNA of each cell type in rat cortex sequencing data. Unpaired *t*-tests were performed for comparison between each neuronal cell type and each non-neuronal cell type individually (****, $P \leq 0.0001$). (**E**) Expression patterns of the *Rbfox3* genes in clusters of rat cortex cells. (**F**) Violin plots showing the n-counts-RNA of each cell type in goat retina and optic nerve sequencing data. Unpaired *t*-tests were performed for each neuronal cell type compared to each non-neuronal cell type individually (****, $P \leq 0.0001$). SST Ins, somatostatin inhibitory neurons; PV Ins, parvalbumin inhibitory neurons; OPC, oligodendrocyte precursor cell.

Investigative Ophthalmology & Visual Science

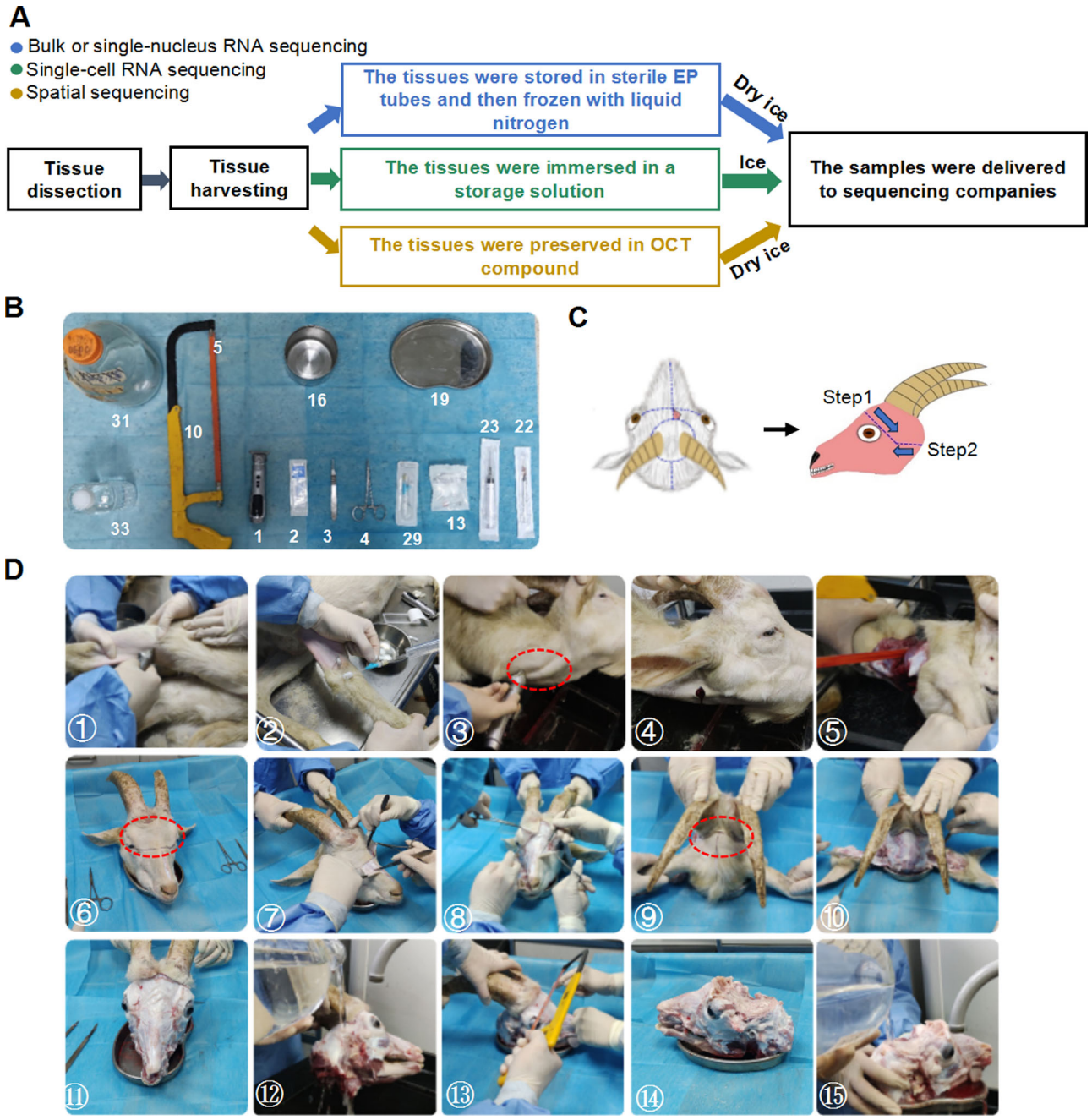


**Figure 4.** Dissection process for multi transcriptomic sequencing sample collection from the goat optic nerve. (**A**) Schematic illustration of the tissue processing and preservation methods for different sequencing types. (**B**) Surgical tools and equipment used for tissue dissection from goat optic nerves. Detailed information is shown in Table 2. (**C**) Schematic of tissue dissection. The *left panel* illustrates the skin incision prior to skin removal, whereas the *right panel* shows the direction and sequence of the saw lines used to remove the skull roof bone. (**D**) Step-by-step photographic sequence of the tissue dissection to expose optic nerve and optic chiasm. Steps 1 to 4: Euthanizing the goat. The *red circle* indicates the external jugular vein. Step 5: Using a saw to separate the body from the head. Steps 6 to 11: Peeling the skin from the goat's head. The *red circle* indicates the skin incision prior to skin removal. Step 12: Flashing the head of the goat with DEPC-treated PBS. Steps 13 and 14: Removing the goat's skull roof bone. Step 15: Flashing the head of the goat with DEPC-treated PBS.

## Quality Assessment of the Extracted RNA for Different Transcriptomic Analyses

The aforementioned tissue harvesting process resulted in high RNA quality extracted from the optic nerve in both large animals and postmortem humans.

In bulk sequencing, the average A260/280 ratios of the optic nerve and retina were 1.87 ± 0.06 and 1.98 ± 0.02, respectively (Fig. 7A). According to literature, an A260/280 ratio exceeding 1.8 is generally viewed as an acceptable indicator of high-quality RNA.[14] We further used the RNA Integrity Number (RIN) and RNA electropherograms to assess RNA integrity and degradation.[15,16] We found that the average RIN values for the retina and optic nerve were 7.97 and 6.8, respectively, indicating that the mRNA extracted from the retina was of higher quality than that from the

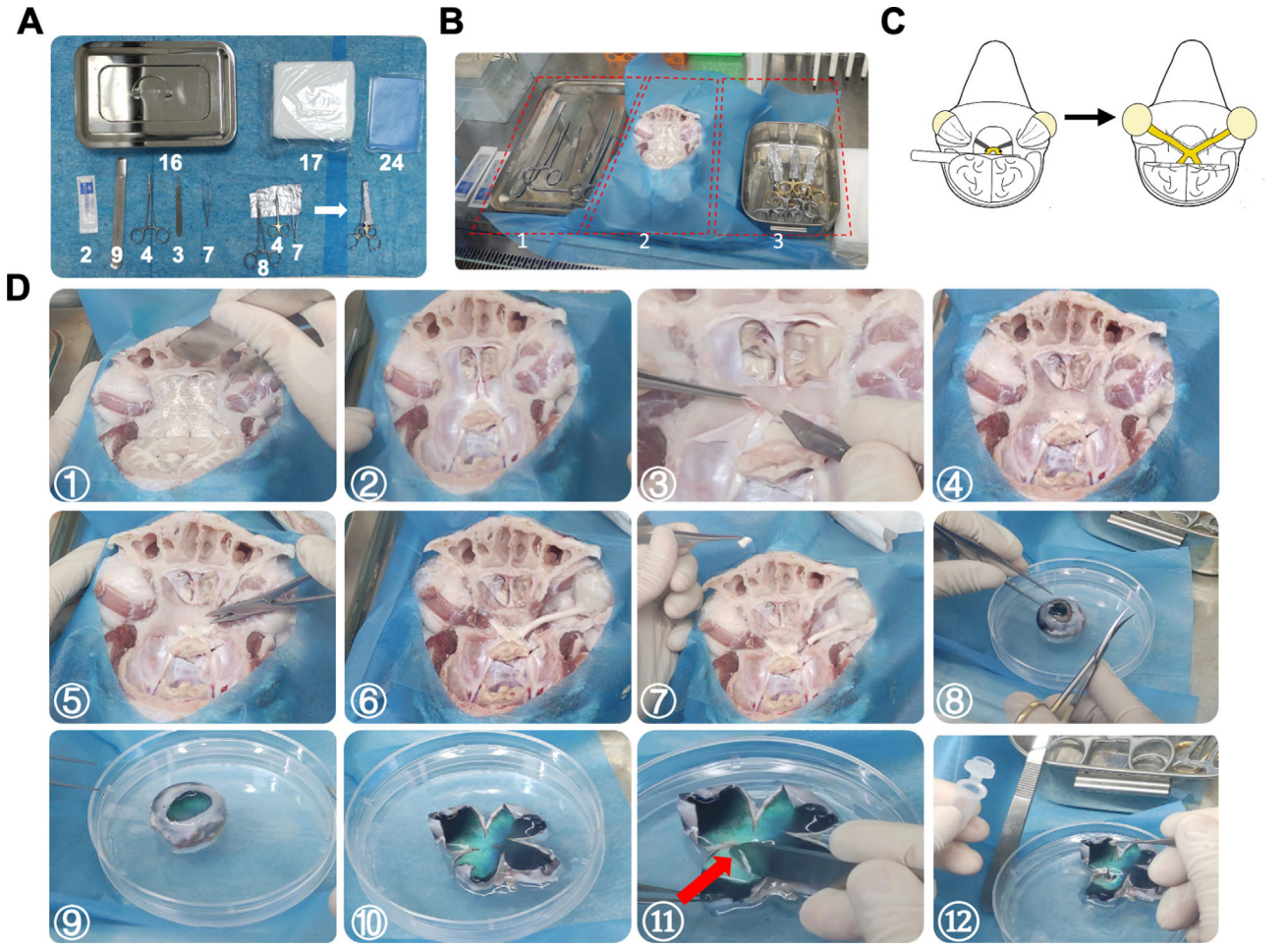


**Figure 5.** Isolation procedures for obtaining optic nerve and retina samples from goats. (**A**) Surgical equipment for harvesting the optic nerve and retina. Detailed information is shown in Table 3. (**B**) The ultraclean table was organized into three designated areas for tissue harvesting. Area 1 held common instruments that did not directly contact the samples, placed to the left of the exposed skull; and area 2 was reserved for the goat head. The exposed skull was covered with a disposable surgical drape, leaving only the sampling area visible; area 3 contained specific instruments for tissue harvesting, positioned to the right of the exposed skull. (**C**) Diagrams showing the process of exposing tissue, including the optic nerve and eyeballs. (**D**) Step-by-step photographic sequence of tissue harvesting for goat optic nerve and retina. 1 and 2: Removal of brain tissue. 3 and 4: Stripping of the periosteum. 5 and 6: Removal of the skull above the intra-orbital and intra-canalicular optic nerve. 7 and 8: Collection of samples, including the optic nerve and eyeball. 9 and 12: Process of acquiring the retina from the eye. The *red arrows* indicate scraped retinas.

optic nerve, likely due to higher mRNA expression in the retina (see Fig. 7A). The 28S:18S peak area under the curve (AUC) ratio in the RNA electropherograms was greater than or equal to 2, indicating good RNA integrity (Fig. 7B). For single nucleus sequencing of human optic nerve samples, our process also yielded high-quality RNA, with an average RIN value of 8.33 ± 0.23 (Fig. 7C).

For single-cell RNA sequencing, cell viability is crucial. We optimized the tissue dissociation process to ensure high-quality single-cell suspensions. Initially, collagenase digestion for 30 minutes yielded low cell viability (Fig. 7D). The optimized 2-step method—collagenase for 30 minutes, then trypsin for 10 minutes—tripled cell density and achieved a 93% ± 1.83 survival rate (see Fig. 7D).

For spatial sequencing samples from goat optic nerves, the average RIN was 8.33 ± 0.23 (Fig. 7E). Interestingly, spatial sequencing exhibited significantly higher RIN values compared to bulk RNA-sequencing, likely due to tissue sectioning and enhanced preservation at low temperatures combined with OCT protection (see Fig. 7E). To maximize the extraction of nucleic acids from the optic nerve, we optimized the RNA permeabilization time for spatial sequencing. The results showed that a permeabilization time of 12 minutes was sufficient to extract mRNA from normal goat optic nerves (Fig. 7F).

## Discussion

### Procedural Considerations and Troubleshooting

While preparing a goat's optic nerve, various challenges may arise. Each step presents potential pitfalls. For RNA extraction, we use a combination of DEPC and RNase Knockout solution. DEPC inhibits RNase, protecting the RNA, whereas RNase Knockout solution is composed of RNase-free reagents and can reliably prevent RNA degradation during RNA extraction and handling.[17]

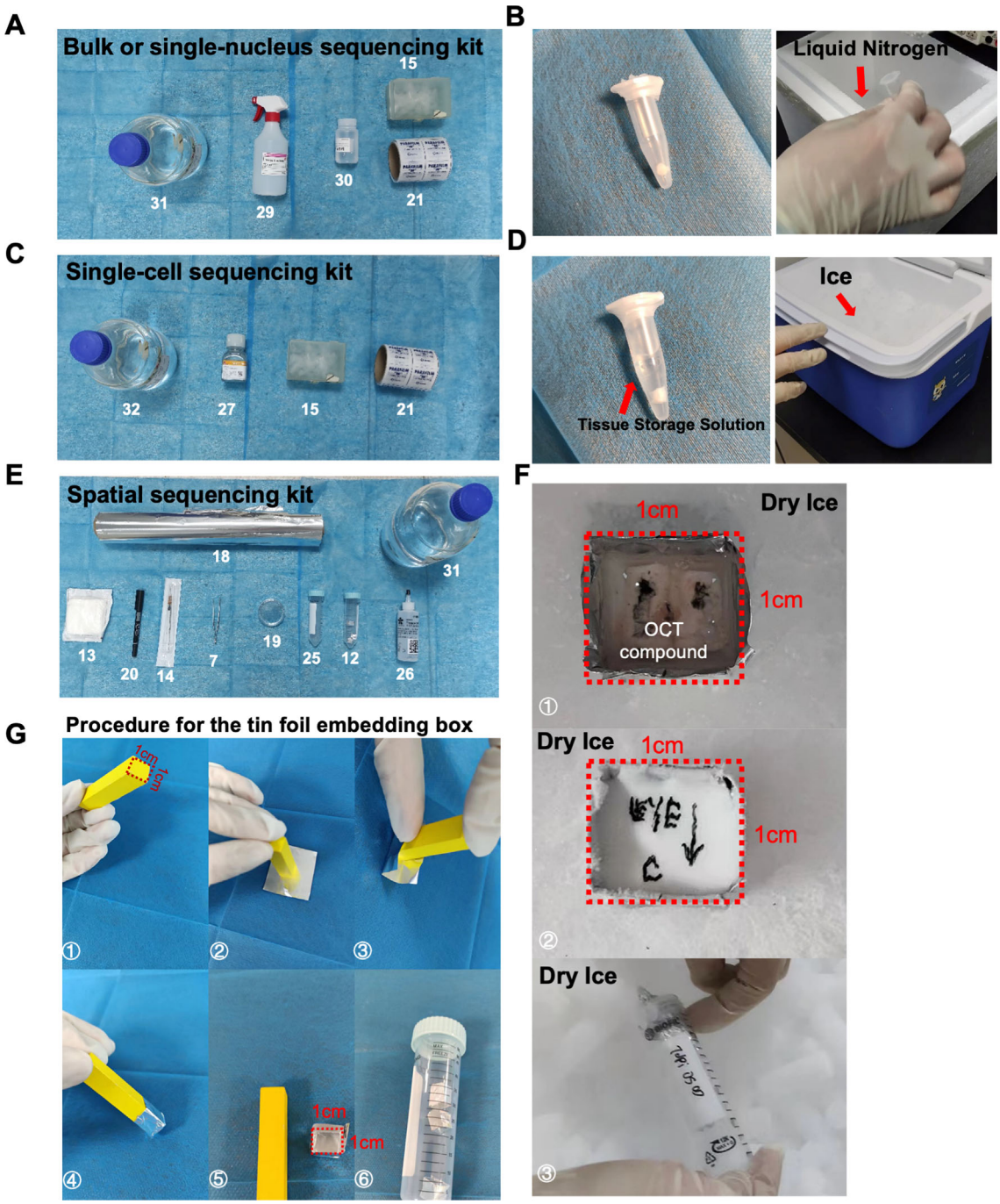


**Figure 6.** Collection and preservation of multi-transcriptomic samples. (**A**) Bulk or single-nucleus sequencing kit showing the necessary materials used for sample preparation. Detailed information is shown in Table 4. (**B**) Images demonstrate the frozen state and conditions of bulk RNA-sequencing and single-nucleus RNA sequencing samples. (**C**) Single-cell RNA sequencing kit showing the tools and reagents used for preparing single-cell samples. Detailed information is provided in Table 4. (**D**) Images demonstrate the frozen state and conditions of single-cell RNA sequencing samples. (**E**) Spatial sequencing kit showing tools used for spatial sequencing embedding. Detailed information is provided in Table 4. (**F**) Schematic of the embedding process for spatial sequencing. (**G**) Step-by-step procedure for creating the 1 cm × 1 cm base tin foil embedding box for spatial sequencing.

## Low mRNA Distribution in the Optic Nerve

We applied fluorescence in situ hybridization and snRNA-seq, revealing notable differences in neuronal distribution between GM and WM. According to our knowledge, we are the first to report that mRNA expression in WM is significantly lower than that in GM. In the goat cortex, we saw notable mRNA expression differences between *Rbfox3*-positive and *Rbfox3*-negative cells (see Figs. 1C, 1D). Across multiple species and tissues, snRNA-seq consistently showed that neuronal cells contain more mRNA than non-neuronal cells (see Fig. 3). However, certain discrepancies arose between the two methods. The in situ hybridization was conducted using tissue sections where the cell structure

**A**

Quality assessment of bulk RNA sequencing

| Goat sample | A260/A280 | Rin |
|---|---|---|
| Optic nerve 1 | 1.94 | 6.2 |
| Optic nerve 2 | 1.95 | 7.3 |
| Optic nerve 3 | 1.74 | 6.9 |
| Retina 1 | 1.95 | 7.5 |
| Retina 2 | 2.03 | 8.2 |
| Retina 3 | 1.97 | 8.2 |

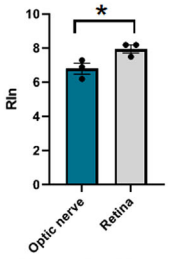


**B**

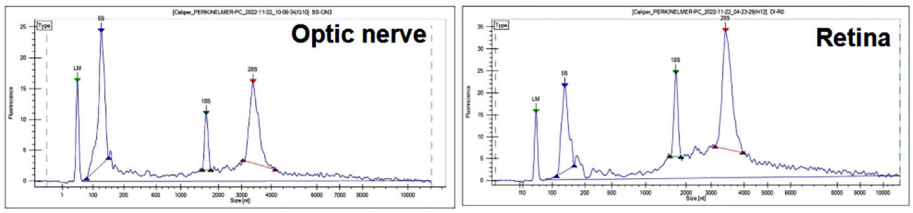


**C**

Quality assessment of single-nucleus RNA sequencing

| Human sample | Rin |
|---|---|
| Optic nerve 1 | 8.6 |
| Optic nerve 2 | 8.6 |
| Optic nerve 3 | 7.7 |

**D**

Quality assessment of single-cell RNA sequencing

| Goat sample | Estimated total cell count | Cell density (per μl) | Cell viability (%) | Agglomeration rate (%) |
|---|---|---|---|---|
| Optic nerve 4 (unoptimized) | 2.0E+04 | 420 | 87 | 5.9 |
| Optic nerve 5 (optimized) | 1.0E+05 | 1620 | 96.7 | 6.7 |
| Optic nerve 6 (optimized) | 1.0E+05 | 1650 | 91 | 5.3 |
| Optic nerve 7 (optimized) | 1.0E+05 | 1370 | 91.4 | 4.1 |

**E**

Quality assessment of spatial sequencing

| Goat sample | Slice thickness (μm) | Rin |
|---|---|---|
| Optic nerve 8 | 10 | 7.9 |
| Optic nerve 9 | 10 | 8.4 |
| Optic nerve 10 | 10 | 8.7 |

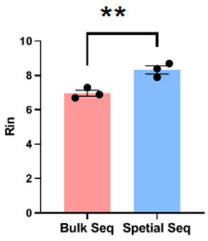


**F**

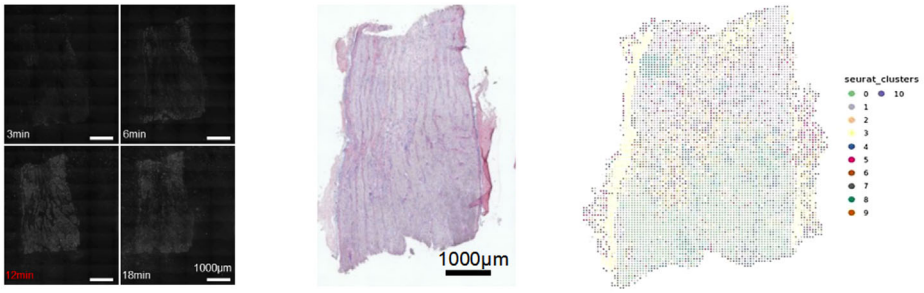


**Figure 7.** Quality control results for the multi-transcriptomic samples of goats. (**A**) *Left panel*: quality assessment results for bulk RNA-sequencing of the goat optic nerve and retina samples. *Right panel*: quantitative analyses of the RIN values between goat retina and optic nerve samples. Error bars indicate the standard error. Significance scores represent *P* values of unpaired *t*-tests (*, $P < 0.05$). (**B**) Representative RNA electropherograms of goat optic nerve and retina samples from bulk RNA-sequencing. The peaks of the electropherograms indicate LM (marker), 5S rRNA, 18S rRNA, and 28S rRNA. (**C**) Quality assessment of single-nucleus RNA sequencing for human optic nerve samples. (**D**) Quality assessment of single-cell RNA sequencing for goat optic nerve samples. (**E**) *Left panel*: quality assessment of spatial sequencing for goat optic nerve samples. *Right panel*: quantitative analyses of the RIN values between bulk RNA-sequencing and spatial sequencing in goat optic nerve samples. Error bars indicate the standard error. Significance scores represent *P* values of unpaired *t*-tests (**, $P < 0.01$). (**F**) The *left panel* shows the different permeabilization times of the goat optic nerve in the tissue optimization experiment; the best permeabilization time was 12 minutes. Scale bars represent 1000 μm. The *middle panel* displays a H&E-stained image of a 10 μm section of the goat optic nerve. The scale bar indicates 1000 μm. The right panel shows the initial clustering plot of the spatial transcriptome profile of the goat optic nerve. H&E, hematoxylin and eosin.

remains intact. In contrast, snRNA-seq involves the extraction of cell nuclei, which may not capture cytoplasmic mRNA, potentially leading to smaller difference in mRNA expressing between GM and WM (see Fig. 1, Supplementary Fig. S1).

Given the importance of neuronal cells in guiding neuronal axons and dendrites, as well as regulating protein generation and synaptic activity, sufficient mRNA is needed in the neuronal soma for downstream activities.[18,19] Although evidence suggests that proteins can be synthesized and transported in axons, the exact distribution of ribosomes in axons and whether there are structures equivalent to the rough endoplasmic reticulum and Golgi apparatus are unclear, indicating that local mRNA expression in axons may not play a predominant role within neuronal cells.[18] We found lower mRNA expression in the optic nerve than in the GM may have been due to low mRNA expression in non-neuronal cells within the optic nerve itself and relatively low mRNA expression within neuronal axons.

### Further Optimization of Dissociation Efficiency

High cell viability is crucial for assessing the quality of single-cell transcriptomes. Our experiments on optic nerve tissue samples showed cell viability similar to that of human retina samples,[20,21] indicating the efficacy of our method. However, the rate of agglomeration of the optic nerve remained high (see Fig. 7D), presumably due to incomplete tissue digestion or cell adhesion caused by the release of DNA. Additional complex enzyme combination schemes may be required to enhance the dissociation efficiency for hard to digest tissues.[22] We optimized enzyme combinations and found that a dual-enzyme protocol resulted in better cell numbers and viability than did collagenase-only digestion (see Fig. 7D). Nevertheless, there is still room for improvement to obtain single-cell suspensions.

### Animal Age Selection and its Impact on Experimental Outcomes

In this study, we utilized 2-month-old rats and 8-month-old goats, both of which are categorized as young adults in their respective species. This age selection was intentional to minimize the influence of age-related factors on our findings. Aging is often associated with alterations in gene expression, potentially leading to mRNA level change in response to neurodegenerative processes.[1,23,24] Dissection procedures may become more challenging with older animals due to anatomic and physiological changes, such as increased tissue fragility and potential degeneration. Although we did not conduct experiments on aged animals, we acknowledge the necessity of addressing these challenges in future studies that investigate age-dependent changes.

### Applications in Studying Post-Injury Transcriptomic Responses

The present study demonstrates that our optimized RNA extraction protocol is effective for analyzing mRNA levels in the optic nerve of large animal models.[5] Importantly, this protocol offers substantial potential for investigating post-injury responses across various injury and disease models. Utilizing this methodology, we identified elevated mRNA expression levels (Supplementary Fig. S3) and transcriptomic changes mainly enriched in pathways related to inflammation, ischemia, and metabolism in the optic canal crush injury model.[5] Our protocol enables the precise dissection and high-quality RNA extraction necessary to capture these dynamic changes. By facilitating the study of temporal dynamics of mRNA expression, our research program can help researchers further explore the potential mechanisms of optic nerve repair and regeneration.

In summary, our protocol effectively addresses low mRNA expression in WM and serves as a robust tool for studying the complex molecular responses after optic neuropathy.

## *Acknowledgments*

The authors express their gratitude to all the donors and their families.

Supported by the National Key R&D Program of China (2022YFA1105500), the National Natural Science Foundation of China (82171048 and 81800842), the Key R&D Program of Zhejiang Province (2021C03065), the Key R&D Program of Wenzhou Eye Hospital (YNZD1201902), the Key R&D Program of Wenzhou (ZY2022021) and the R&D Program of Wenzhou (H20220008), and the National Key R&D Program of China (2018YFA0701703).

Disclosure: **Z. Yu**, None; **Y. Guan**, None; **T. Xia**, None; **X. Li**, None; **M. Liu**, None; **Y. Huo**, None; **Z. Wang**, None; **Z. Liu**, None; **Y. Luo**, None; **W. Yan**, None; **L. Sun**, None; **W. Wu**, None; **B. Shen**, None; **Y. Zhang**, None

## *References*

1. Hou Y, Dan X, Babbar M, et al. Ageing as a risk factor for neurodegenerative disease. *Nat Rev Neurol*. 2019;15(10):565–581.
2. Gorman AM. Neuronal cell death in neurodegenerative diseases: recurring themes around protein handling. *J Cell Mol Med*. 2008;12(6a):2263–2280.
3. Ghaffarieh A, Levin LA. Optic nerve disease and axon pathophysiology. *Int Rev Neurobiol*. 2012;105:1–17.
4. Levin LA, Beck RW, Joseph MP, Seiff S, Kraker R. The treatment of traumatic optic neuropathy: the International Optic Nerve Trauma Study. *Ophthalmology*. 1999;106(7):1268–1277.
5. Zhang Y, Li M, Yu B, et al. Cold protection allows local cryotherapy in a clinical-relevant model of traumatic optic neuropathy. *Elife*. 2022;11:e75070.
6. Vrentas CE, Boggiatto PM, Schaut RG, Olsen SC. Collection and processing of lymph nodes from large animals for RNA analysis: preparing for lymph node transcriptomic studies of large animal species. *J Vis Exp*. 2018;(135):57195, doi:10.3791/57195.
7. Tao Y, Zhou X, Sun L, et al. Highly efficient and robust $\pi$-FISH rainbow for multiplexed in situ detection of diverse biomolecules. *Nat Commun*. 2023;14(1):443.
8. Karayannis T, Au E, Patel JC, et al. Cntnap4 differentially contributes to GABAergic and dopaminergic synaptic transmission. *Nature*. 2014;511(7508):236–240.
9. Hu C, Li T, Xu Y, et al. CellMarker 2.0: an updated database of manually curated cell markers in human/mouse and web tools based on scRNA-seq data. *Nucleic Acids Res*. 2023;51(D1):D870–D876.
10. Kim KK, Adelstein RS, Kawamoto S. Identification of neuronal nuclei (NeuN) as Fox-3, a new member of

the Fox-1 gene family of splicing factors. *J Biol Chem*. 2009;284(45):31052–31061.
11. Mullen RJ, Buck CR, Smith AM. NeuN, a neuronal specific nuclear protein in vertebrates. *Development*. 1992;116(1):201–211.
12. Passmore LA, Coller J. Roles of mRNA poly(A) tails in regulation of eukaryotic gene expression. *Nat Rev Mol Cell Biol*. 2022;23(2):93–106.
13. Polasek M, Yang Y, Schühle DT, et al. Molecular MR imaging of fibrosis in a mouse model of pancreatic cancer. *Sci Rep*. 2017;7(1):8114.
14. Nielsen H. Working with RNA. *Methods Mol Biol*. 2011;703:15–28.
15. Schroeder A, Mueller O, Stocker S, et al. The RIN: an RNA integrity number for assigning integrity values to RNA measurements. *BMC Mol Biol*. 2006;7:3.
16. Fleige S, Pfaffl MW. RNA integrity and the effect on the real-time qRT-PCR performance. *Mol Aspects Med*. 2006;27(2-3):126–139.
17. Chomczynski P. Solubilization in formamide protects RNA from degradation. *Nucleic Acids Res*. 1992;20(14):3791–3792.
18. Mofatteh M. mRNA localization and local translation in neurons. *AIMS Neurosci*. 2020;7(3):299–310.
19. Fonkeu Y, Kraynyukova N, Hafner A-S, et al. How mRNA localization and protein synthesis sites influence dendritic protein distribution and dynamics. *Neuron*. 2019;103(6):1109–1122.e7.
20. Eriksen AZ, Møller R, Makovoz B, et al. SARS-CoV-2 infects human adult donor eyes and hESC-derived ocular epithelium. *Cell Stem Cell*. 2021;28(7):1205–1220.e7.
21. Lu Y, Shiau F, Yi W, et al. Single-cell analysis of human retina identifies evolutionarily conserved and species-specific mechanisms controlling development. *Dev Cell*. 2020;53(4):473–491.e9.
22. Leelatian N, Doxie DB, Greenplate AR, et al. Single cell analysis of human tissues and solid tumors with mass cytometry. *Cytometry B Clin Cytom*. 2017;92(1):68–78.
23. Hahn O, Foltz AG, Atkins M, et al. Atlas of the aging mouse brain reveals white matter as vulnerable foci. *Cell*. 2023;186(19):4117–4133.e22.
24. Cai Y, Song W, Li J, et al. The landscape of aging. *Sci China Life Sci*. 2022;65(12):2354–2454.

Investigative Ophthalmology & Visual Science